Manuscript Title: Mass spectrometry imaging of natural carbonyl products directly from agar-based microbial interactions using 4-APEBA derivatization

Running title: Direct imaging of carbonyls in microbial interactions

Authors: Dušan Veličković,[a]* Kevin J. Zemaitis,[a]* Arunima Bhattacharjee,[a] Christopher R. Anderton[a]

Affiliation: Environmental Molecular Sciences Laboratory, Pacific Northwest National Laboratory, Richland, WA 99354[a]

*Address correspondence to Dušan Veličković, dusan.velickovic@pnnl.gov; Kevin J. Zemaitis, kevin.zemaitis@pnnl.gov

ABSTRACT

Aliphatic carboxylic acids, aldehydes, and ketones play diverse roles in microbial adaptation to their microenvironment, from excretion as toxins to adaptive metabolites for membrane fluidity. However, the spatial distribution of these molecules throughout biofilms, and how microbes in these environments exchange these molecules remains elusive for many of these bioactive species due to non-efficient molecular imaging strategies. Herein, we apply on-tissue chemical derivatization (OTCD) using 4-(2-((4-bromophenethyl)dimethylammonio)ethoxy)benzenaminium bromide (4-APEBA) on a co-culture of a soil bacterium (*Bacillus subtilis* NCIB 3610) and fungus (*Fusarium* sp. DS 682) grown on agar as our model system. Using matrix-assisted laser desorption/ionization mass spectrometry imaging (MALDI-MSI), we spatially resolved more than 300 different metabolites containing carbonyl-groups within this model system. Various spatial patterns are observable of these species, which indicate possible extracellular or intercellular processes of the metabolites, and their up or down regulation during microbial interaction. The unique chemistry of our approach

allowed us to bring additional confidence in accurate carbonyl identification, especially when multiple isomeric candidates were possible, and this provided the ability to generate hypotheses about the potential role of some aliphatic carbonyls in this *B. subtilis*/*Fusarium* sp. interaction. The results shown here demonstrate the utility of 4-ABEBA-based OCTD MALDI-MSI in probing interkingdom interactions directly from microbial co-cultures, and these methods will enable future microbial interactions studies with expanded metabolic coverage.

IMPORTANCE

The metabolic profiles within microbial biofilms and interkingdom interactions are extremely complex and serve a variety of functions, which include promoting colonization, growth, and survival within competitive and symbiotic environments. However, measuring and differentiating many of these molecules, especially in an *in-situ* fashion, remains a significant analytical challenge. We demonstrate a chemical derivatization strategy that enabled highly sensitive, multiplexed mass spectrometry imaging of over 300 metabolites from a model microbial co-culture. Notably, this approach afforded us to visualize over two dozen classes of ketone-, aldehyde-, and carboxyl-containing molecules, which were previously undetectable from colonies grown on agar. We also demonstrate that this chemical derivatization strategy can enable discrimination of isobaric and isomeric metabolites, without the need for orthogonal separation (*e.g.,* online chromatography or ion mobility). We anticipate this approach will further enhance our knowledge of metabolic regulation within microbiomes and microbial systems used in bioengineering applications.

KEYWORDS

MALDI, metabolomics, carboxylic acids, aldehydes, ketones, *Bacillus subtilis*, *Fusarium*

INTRODUCTION

Mass spectrometry imaging (MSI) is becoming an established technique for exploring the nature and diversity of the chemical compounds produced in microbial systems (1-3). It has been extensively applied in understanding biochemical processes in microbial and host-microbe interactions (2), biofilm formation (4), and microbial phenotyping (5). Within literature, spatial probing via MSI for retrieving localized metabolic signatures is commonly performed on microbial systems grown on agar or other solid growing medium, including other organisms (6). While there are numerous types of ionization modalities and mass spectrometry approaches such as nanospray desorption electrospray ionization (nanoDESI) (7), laser ablation electrospray ionization (LAESI) (8), liquid extraction surface analysis (LESA) (9), and ultrahigh lateral resolution secondary ion mass spectrometry (SIMS) (10) that have been used to chemically image microbial samples, matrix-assisted laser desorption/ionization (MALDI) methods are most broadly implemented, in part, due to their robustness, reproducibility, high spatial resolution, and wide molecular coverage (1, 11-14).

While there are many classes of metabolites and small molecules that can be readily detected and annotated by MALDI-MSI (14), the ability to obtain comprehensive detection of natural acidic compounds, including aliphatic carboxylates and carbonyls, which play diverse roles in microbes (15-18), and are valuable additives in food, fragrances, and pharmaceuticals (15, 16), remains a significant challenge. For example, MALDI-MSI analyses of agar-based samples has been limited to the positive ionization modality where these classes of

67 biomolecules ionize poorly. The sparse reporting of negative ionization mode analyses is
68 presumed to be ascribed to the chemistry of the agar, which has a negative charge due to
69 sulfate groups. This could dissipate charge during negative ion mode analysis, and/or possibly
70 limit the ability of MALDI matrices used in negative ionization mode to efficiently extract and
71 co-crystalize with analytes on the agar surface. Perhaps this is, in part, a reason why others
72 developed imprinting strategies to transfer colonies from agar to more suitable supports for
73 negative ionization mode analysis (19). Nevertheless, even imprinting approaches have
74 limitations, where transfer efficiency, molecular selectivity, and molecular relocation are
75 notable issues for comprehensive molecular mapping (20).

76 Here, we provide a new MSI approach for mapping endogenous metabolites containing
77 carbonyl groups from microbial systems. We applied our previously developed on-tissue
78 chemical derivatization (OTCD) protocol to microbial cultures grown on agar as a proof-of-
79 concept of this approach (21). There are a growing number of OTCD reagents and protocols
80 that have been developed to increase the sensitivity and molecular coverage from mammalian
81 and plant samples in MALDI-MSI (22-24). Our approach uses 4-(2-((4-
82 bromophenethyl)dimethylammonium)ethoxy)benzenaminium dibromide (4-APEBA), which
83 adds a permanent positive charge to carbonyl analytes, making them amenable to positive
84 ionization mode analysis MSI, which is especially useful for analyzing agar-based microbial
85 colonies. Additionally, the bromine in 4-APEBA introduces a unique isotopic pattern to
86 derivatized molecules, which can be exploited for more confident analyte annotation (21). We
87 used this approach to study the interaction of soil microbes *B. subtilis* NCIB 3610 and *Fusarium*
88 sp. DS 682 (25). Our results demonstrate that this approach enabled high-sensitivity analysis of

89 over 300 microbially generated carbonyl-containing molecules directly from microbial cultures
90 on agar plates. To our knowledge, this is the first demonstration of using an OTCD approach for
91 MSI-based metabolic profiling of microbial systems.

92 **RESULTS AND DISCUSSION**

93 Our results show that 4-APEBA-based OTCD of the *B. subtilis* NCIB 3610 and *Fusarium*
94 sp. DS 682 interaction enabled confident chemical formula annotations of over 300 various
95 carbonyls, which putative structural annotations are proposed in **Supplementary Table S1** and
96 are further classified in **Supplementary Figure S1**. In comparison, when we analyzed sample
97 replicates without OTCD, in the negative ionization mode, less than ten annotated molecular
98 formulae were annotated with high confidence, and the list of annotations can be found on
99 METASPACE (26). This comparison clearly demonstrates the necessity of alternative approaches
100 for carbonyl detection from agar samples.

101 In the 4-APEBA-based OTCD analysis, several spatial patterns that depict changes in
102 specific metabolite production between isolated and interacting microbes were observed
103 (**Figure 1**). For example, we identified a group of molecules produced and excreted by *B. subtilis*
104 only in its interaction with *Fusarium* sp. (*e.g.*, hexosamine, **Figure 1B**). Conversely, the
105 production of an *N*-acetylated form of hexosamine (likely *GlcNAc*) was triggered in *Fusarium*
106 sp., but not *B. subtilis*, with the interaction of these two species (**Figure 1E**). This finding is
107 congruent with previous reports that *GlcNAc* acts as a signal inducer within fungi and also
108 serves in interkingdom communication (27). Contrasting spatial distributions were observed
109 with citrate and homocitrate (**Figure 1C and 1F**, respectively), which are two chemically and

110 metabolically related molecules. We observed homocitrate to be produced only in isolated *B.*
111 *subtilis* colonies, while citrate, a central metabolite of the TCA cycle (28), was produced in both
112 isolated and interacting *Fusarium* sp.. Based on citrate co-localization with *B. subtilis* cells only
113 in the interaction zone, we hypothesize that citrate originating from *Fusarium* sp. might serve
114 as a carbon source for adjacent *B. subtilis* colonies during the interaction. Our MSI data also
115 found that other carbonyls have a variety of unique spatial patterns, including those:
116 unchanged during interaction (*e.g.*, succinyl-glutamate, **Figure 1D**), present in distinct
117 phenotypes of in the *B. subtilis* biofilm (*e.g.*, acetyl-citrulline, **Figure 1G**), suppressed in both
118 species when interacting (*e.g.*, aminobutanoate, **Figure 1H**), and activated in both species in
119 their interactions (*e.g.*, acetamidopentanoate, **Figure 1E**). A list of all other metabolites
120 annotated, together with their discriminant coefficients (AUC) between isolated and interacted
121 species, can be found in **Supplementary Table S1.**

122 Besides homocitrate (**Figure 1C**), citrate (**Figure 1F**), and several dozen other
123 polycarboxylic acids (**Supplementary Table S1)**, we annotated numerous aliphatic
124 monocarboxylic acids (*i.e.*, free fatty acids; FFA) as 4-APEBA derivatives (**Figure 2**). Their spatial
125 profile points to the different roles of these molecules during the *B. subtilis* and *Fusarium* sp.
126 interaction. For example, there is intense excretion of short-chain FFA (**Figure 2A-B**) from *B.*
127 *subtilis* during interaction with *Fusarium* sp.. In contrast, medium-chain FFA (C14-C16, **Figure**
128 **2C-E**) are colocalized with *B. subtilis* cells further from the interaction zone. It is known that
129 *Bacillus* spp. can modify their FFA patterns to adapt to a wide range of environmental changes
130 (29), and based on our results, it seems that the production of short-chain FFA is vital for
131 surviving in a *Fusarium* sp. environment. On the other hand, *Fusarium* sp., in interaction with *B.*

132 *subtilis* boosts the production of long chain FFA (C18, **Figure 2F-H**). This reinforced production
133 of long-chain FFA might be related to the antimicrobial defense mechanisms of *Fusarium* sp..
134 Namely, the antibacterial properties of FFA are used by many organisms, where the prime
135 target of FFA action is the bacterial cell membrane, where FFA disrupts the electron transport
136 chain and oxidative phosphorylation (30). Optical microscopy images of co-cultured *B. subtilis*
137 NCIB 3610 and *Fusarium* sp. DS 682 demonstrate an antagonistic interaction as there is reduced
138 fungal growth in presence of *B. subtilis* compared to the control (**Supplementary Figure S2**). *B.*
139 *subtilis* is known to protect host plants by decreasing pathogenic fungal or bacterial growth
140 through production of secondary metabolites (31), and as the majority of these compounds
141 contain carbonyls, 4-APEBA-based OTCD enables the sensitive tracing of their redistribution and
142 kinetics.

143 Besides comprehensive carbonyl coverage, the additional value of this approach is the
144 ability to confidently resolve some isomeric and isobaric metabolites (**Figure 3**) that are
145 undistinguishable in typical MALDI-MSI experiments, which only provides accurate mass
146 measurements without gas phase separation by ion-mobility. **Figure 3A** shows a MALDI-MS ion
147 image of a brominated derivative product ion at *m/z* 560.1754, illustrating that this metabolite
148 is concentrated on the *B. subtilis* biofilm layer further from the interaction zone. Based on the
149 accurate mass measurements, this ion, within a 3 ppm window, can be ascribed to the
150 derivatized forms of either kinetin ($C_{10}H_9N_5$) or succinyl proline ($C_9H_{13}NO_5$). Both molecules are
151 naturally present in soil (*e.g.*, as a plant hormone and common amino acid, respectively). Since
152 kinetin does not possess a carbonyl group that can be derivatized with 4-APEBA, it suggests that
153 this ion corresponds to succinyl proline as succinyl proline contains multiple carbonyl groups

154 (**Figure 3C**). Interestingly, upregulation of succinylation is a known phenomenon in *B. subtilis*
155 response to carbon source changes, especially when citrate becomes the carbon source (32).
156 This succinylation-citrate relationship orthogonally validates our previous hypothesis that
157 *Fusarium* sp. produces citrate (**Figure 1F**), which is further metabolized by *B. subtilis*.

158 The second example of resolving isobars with 4-APEBA-based OTCD illustrates the
159 importance of using bromine as a non-leaving moiety of the derivatization agent (**Figure 3B**).
160 Namely, bromine has two stable isotopes (^{79}Br and ^{81}Br) with similar relative abundances (51%
161 and 49%, respectively), producing an easily recognizable isotopic pattern, where the
162 monoisotopic (M+0; ^{79}Br) and second isotopologue (A+2; ^{81}Br) peaks have similar intensities.
163 For instance, the ion at *m/z* 494.1471 can be wrongly annotated as methionine (M+0; ^{79}Br
164 derivative) but is actually an isotopologue of glutamate (A+2; ^{81}Br derivative). If this were
165 methionine, an A+2 isotopologue at *m/z* 496.1455 would have a similar intensity as the putative
166 monoisotopic peak at *m/z* 494.1471 (**Figure 3D**), which was not the case. Instead, the peak at
167 *m/z* 492.1492 has the same intensity and exact spatial localization as *m/z* 494.1471, indicating
168 glutamate was derivatized.

169 Lastly, the two-step 4-APEBA-based OTCD approach could be utilized to also
170 differentiate some carbonyl isomers (**Figure 4**). This is because if 4-APEBA is used alone,(33)
171 then it can only derivatize aldehydes and ketones, and it will not derivatize carboxylic acids (21).
172 EDC must be used as an activator for 4-APEBA to derivatize carboxylic acids.(34) As such, we
173 performed 4-APEBA-based OCTD with and without EDC on replicate samples. Multiple
174 overlapping and unique annotations were observed with side-by-side annotations outputs and
175 ion images are visualized in METASPACE (35), and **Supplementary Table S2**. Overlapping

176 annotations between both conditions (with and without the application of EDC) indicate the
177 presence of a ketone or aldehyde group in the metabolite. Whereas in the case which the
178 annotation was only present when EDC was applied prior to 4-APEBA, annotated molecules
179 contain solely carboxylic acids, and aldehyde and ketone groups are absent from their structure
180 and should not be considered. One example of an ambiguous annotation is the ion image at
181 *m/z* 433.1476 ($C_4H_8O_2$) (**Figure 4A-B**). This molecular formula can correspond to two natural
182 products of bacterial metabolism: butanoic acid and acetoin (3-hydroxy-2-butanone) (**Figure**
183 **4E**). As a similar spatial pattern was observed with (**Figure 4A**) and without (**Figure 4B**) the
184 addition of EDC, this ion image, which indicates intense excretion of the metabolite from *B.*
185 *subtilis*, this metabolite is likely is the ketone, acetoin, because the carboxylic acid, butanoic
186 acid, cannot be derivatized without EDC. This annotation aligns well with the fact that acetoin is
187 a primary catabolic product of *B. subtilis,* which bacteria reuse during the stationary phase
188 when other carbon sources have been depleted (36). Moreover, the ion image at *m/z* 447.1641
189 with a similar spatial pattern was previously annotated as pentanoic acid (**Figure 2A**) and was
190 not detected in the analysis without EDC (34), which orthogonally confirms the absence of
191 butanoic acid in the analyzed sample. Other aliphatic carboxylic acids discussed throughout the
192 manuscript (*i.e.,* FFA and some components of the TCA cycle) were also annotated only if EDC
193 was used as an activator, while oxocarboxylic acids, due to the presence of ketone or aldehyde
194 groups, were annotated without EDC as well (**Supplementary Table S2**). For example, the ion
195 at *m/z* 479.1176 **(Figure 4C-D**) with molecular formula of $C_4H_6O_5$ is malate (two carboxyl
196 groups, no ketone or aldehyde groups) rather than dehydro-threonate (carboxyl and ketone
197 group) as this ion was not detected without EDC treatment (**Figure 4F**).

198 This EDC-guided selectivity of 4-APEBA was additionally confirmed by analysis of several
199 standards with different chemistries. Specifically, citric acid, which solely has carboxyl groups;
200 glyoxalic acid, which has a carboxylic and aldehyde group; hydroxyacetone, which has only a
201 ketone group (analog to acetoin); and pyruvic acid, which has both a carboxylic and ketone
202 group (**Figure 5**). Our results show that citric acid, with no ketone or aldehyde groups, was not
203 derivatized without the activation by EDC. Due to the presence of a ketone in pyruvic acid, and
204 an aldehyde group in glyoxalic acid these oxoacid metabolites were even derivatized without
205 EDC. Furthermore, hydroxyacetone, the demethylated analog of acetoin, which we previously
206 distinguished from its isobar butanoic acid, shows clear isotopic patterns corresponding to its 4-
207 APEBA derivatized product.

208 **CONCLUSIONS**

209 Mapping redistribution of acidic compounds in the microbial ecosystem using MALDI-
210 MSI is a significant bioanalytical challenge. This challenge is further exacerbated for microbial
211 cultures on agar, because many of these metabolites readily ionize in negative ionization mode
212 which is not suitable for this type of sample. This work demonstrates a new approach for
213 spatially profiling a diverse set of carbonyls, from small volatile aldehydes, ketones, and short-
214 chain FFA to long-chain aliphatic carboxylic acids, including lactones and oxocarboxylic acids,
215 directly from microbial cultures using 4-APEBA-based OTCD and MALDI-MSI. From our proof-of-
216 concept experiments, we were able to map and reveal the distribution of carbonyls resulting
217 from the interaction of *B. subtilis* and *Fusarium* sp. cultured on agar. These results illustrate the
218 potential role of citrate, hexosamines, and FFA in this interaction. The additional advantage of
219 the described OTCD by 4-APEBA, is that it can distinguish some isobaric and isomeric species,

220 especially those with only a carboxyl group and only a ketone or aldehyde group, as well as
221 those that do not have said functional groups at all. This benefit provides greater confidence in
222 the biological interpretation of microbial MSI data. We also envision application of this
223 workflow to map metabolic processes across a broad range of microbiology fields. For example,
224 it can be used to spatially resolve the metabolome of digestive processes of the human gut,
225 where microbiota produce large quantities of aliphatic acids and aldehydes through anaerobic
226 fermentation of dietary fibers, which influences gut-brain communication and brain function
227 (37). Another potential use is in resolving temporal-spatial chemistry of microbiological
228 lignocellulose decay mechanisms where aldehydes, ketones, and carboxylic acids are both main
229 degradation products and enzyme mediators for further lignin decomposition (38).

230 **MATERIAL AND METHODS**

231 **Microbial growth and co-culture preparation**

232 *B. subtilis* NCIB 3610 was cultured as described before (39). Briefly, the strain was
233 cultured on MSgg, a *B. subtilis* biofilm-promoting medium (5 mM potassium phosphate [pH 7];
234 Fisher Scientific, Waltham, MA), 100 mM MOPS (morpholinepropanesulfonic acid [pH 7];
235 Sigma-Aldrich, St. Louis, MO), 2 mM $MgCl_2$ (Fisher Scientific, Waltham, MA), 700 µM $CaCl_2$ (Alfa
236 Aesar, Haverhill, MA), 50 µM $MnCl_2$ (Fisher Scientific, Waltham, MA), 50 µM $FeCl_3$ (Sigma-
237 Aldrich, St. Louis, MO), 1 µM $ZnCl_2$ (Sigma-Aldrich, St. Louis, MO), 2 µM thiamine hydrochloride
238 (Fisher Scientific, Waltham, MA), 0.5 % glycerol (Fisher Scientific, Waltham, MA), and 0.5%
239 glutamate (Sigma-Aldrich, St. Louis, MO). 1.5 % agar (BD) was added to the medium to prepare

240 agar plates using MSgg media, and approximately 5 mL MSgg agar per plate were poured. MSgg
241 agar plates were streaked with *B. subtilis* from frozen stocks and incubated at 28 °C for 15 hr.

242 *Fusarium* sp. DS 682 was cultured as described before (40). Fungi was maintained on
243 potato dextrose agar (PDA) plates at 28 °C. For co-culture experiments a disposable 1.5 mm
244 holepunch (Integra Miltex, York, PA) was used to collect the fungal biomass from a fungal
245 culture PDA agar plate (1 agar plug with fungi) and was placed on the MSgg agar plate. Fungi
246 was grown at 28°C for 5 days. After 5 days of fungal growth, *B. subtilis* was streaked close to the
247 fungal biomass as described above. Agar plates were prepared for MSI analysis after 2 days of
248 bacterial growth at 28°C.

249 Agar areas with isolated and interaction colonies were excised from MSgg agar Petri
250 dishes, placed onto double-sided adhesive copper tape (3-6-1182; 3M United States) adhered
251 to indium tin oxide-coated glass slides (Bruker Daltonics, Billerica, MA), and dried at RT
252 overnight prior to derivatization and analysis.

253 ***In-situ* chemical derivatization and MALDI matrix application**

254 Agar samples were chemically derivatized by either sole application of synthesized 4-
255 APEBA at 2 mg/mL or with a two-step approach: spraying an aqueous solution of EDC (1-ethyl-
256 3-(3-dimethylaminopropyl)carbodiimide; Sigma-Aldrich, St. Louis, MO) at 6 mg/mL first with
257 subsequent application of 4-APEBA at 2 mg/mL using an external syringe pump with the M5-
258 Sprayer (HTX Technologies, Chapel Hill, NC). Spraying parameters were the same for both
259 chemicals: 25 µL/min flow rate, a nozzle temperature of 37.5 °C, four cycles at 3 mm track
260 spacing with a crisscross pattern, a 2 s drying period, 1,200 mm/min spray head velocity, 10 PSI

261 of nitrogen gas, and a 40 mm nozzle height. DHB (2,5-dihydroxybenzoic acid; Sigma-Aldrich, St.
262 Louis, MO) was prepared at a concentration of 40 mg/mL in 70% MeOH and was sprayed at 50
263 µL/min flow rate using the same M5-Sprayer. The nozzle temperature was set to 70 °C, with 12
264 cycles at 3 mm track spacing with a crisscross pattern. A 2 s drying period was added between
265 cycles, a linear flow was set to 1,200 mm/min with 10 PSI of nitrogen gas and a 40 mm nozzle
266 height. This resulted in matrix coverage of ~667 µg/cm^2 for DHB. For negative ion mode
267 experiments NEDC (N-(1-naphthyl)ethylenediamine dihydrochloride; Sigma-Aldrich, St. Louis,
268 MO) was prepared at a concentration of 7 mg/mL in 70% MeOH and was sprayed at 120 µL/min
269 flow rate using the same M5-Sprayer. The nozzle temperature was set to 70 °C, with 8 cycles at
270 3 mm track spacing with a crisscross pattern. A 0 s drying period was added between cycles, a
271 linear flow was set to 1,200 mm/min with 10 PSI of nitrogen gas and a 40 mm nozzle height.
272 This resulted in matrix coverage of ~187 µg/cm^2 for NEDC.

273 **MALDI-MS analysis and data processing**

274 All imaging was performed on a Bruker Daltonics 12T solariX FTICR MS, equipped with a
275 ParaCell, Apollo II dual ESI and MALDI source with a SmartBeam II frequency-tripled (355 nm)
276 Nd: YAG laser (Bremen, Germany). Positive ion mode OTCD and negative ion mode NEDC
277 acquisitions were acquired with broadband excitation from *m/z* 98.3 to 1,000, resulting in a
278 detected transient of 0.5593 s — the observed mass resolution was ~110k at *m/z* 400.
279 FlexImaging (Bruker Daltonics, v.5.0) was used for the imaging experiments, and analyses were
280 performed with a 100 µm step size. FlexImaging sequences were directly imported into SCiLS
281 Lab (Bruker Daltonics, v.2023.a Premium 3D) using automatic MRMS settings. Ion images were
282 directly processed from the profile datasets within SCiLS Lab, and automated annotation of the

283 centroided dataset was completed within METASPACE with a chemical modifier corresponding
284 to the mass shift expected from 4-APEBA derivatization (+$C_{18}H_{22}N_2Br$, +345.0966 Da). KEGG-v1
285 was used as a metabolite database for annotations. All annotations were imported back to
286 SCiLS as a new peak list, and discrimination analysis (ROC, receiver operation characteristic)
287 between species in the interaction and corresponding isolated species were performed on that
288 list. Area under the curve (AUC) of ROC analysis for each pair (isolated microbe vs microbe in
289 interaction) was calculated.

290 **Data availability**

291 All MALDI-MSI datasets and annotations are publicly available at METASPACE, a link for
292 reviewers is here: https://metaspace2020.eu/api_auth/review?prj=b43e6772-d58c-11ed-afbb-
293 53f7af38ceec&token=SVQu4QGZBzO6

294 **SUPPLEMENTAL MATERIAL FILE LIST**

295 The following is included as supplementary material for this manuscript.

296 **Figure S1.** Supplemental file 1 contains this figure that shows the breakdown of assigned
297 carbonyl derivative ions from KEGG-v1 output of METASPACE.

298 **Figure S2.** Supplemental file 1 contains this a figure that shows microscopy images of
299 the growth of the co-cultured *B. subtilis* and *Fusarium* sp. on the MSgg agar medium.

300 **Table S1.** Supplemental file 2 is a complex workbook which shows the discriminate
301 analyses completed for co-cultured *B. subtilis* and *Fusarium* sp. highlighting AUC within the
302 isolated colonies and the interaction zone.

303 **Table S2.** Supplemental file 3 is a complex workbook which highlights all annotations
304 from KEGG-v1 output of METASPACE for experiments with and without application of EDC
305 before 4-APEBA.

306 **ACKNOWLEDGMENT**

307 This research was performed on a project award
308 doi.org/10.46936/intm.proj.2021.60091/60001441 (D.V.) from the Environmental Molecular
309 Sciences Laboratory, a Department of Energy (DOE) Office of Science User Facility sponsored by
310 the Biological and Environmental Research program under Contract No. DE-AC05-76RL01830.
311 The funders had no role in study design, data collection and interpretation, or the decision to
312 submit the work for publication.

313 **AUTHOR CONTRIBUTIONS**

314 D.V. obtained funding and administered the project. D.V. and K.J.Z conceptualized the
315 project. A.B. provided input into the microbiology and performed all microbiological work. A.B.
316 created all cultures. D.V. performed derivatization and all MALDI-MSI experiments. D.V. and
317 K.J.Z. performed data analysis and visualization. D.V. wrote the first draft of the manuscript
318 with inputs from K.J.Z., A.B, and C.R.A. All authors edited the manuscript.

319 **REFERENCES**

320 1. Feucherolles M, Frache G. 2022. MALDI Mass Spectrometry Imaging: A Potential Game-Changer
321 in a Modern Microbiology. Cells 11.
322 2. Dunham SJB, Ellis JF, Li B, Sweedler JV. 2017. Mass Spectrometry Imaging of Complex Microbial
323 Communities. Accounts of Chemical Research 50:96-104.

324 3. Spraker JE, Luu GT, Sanchez LM. 2020. Imaging mass spectrometry for natural products
325 discovery: a review of ionization methods. Natural Product Reports 37:150-162.
326 4. Yannarell SM, Velickovic D, Anderton CR, Shank EA. 2021. Direct Visualization of Chemical Cues
327 and Cellular Phenotypes throughout Bacillus subtilis Biofilms. Msystems 6.
328 5. Stasulli NM, Shank EA. 2016. Profiling the metabolic signals involved in chemical communication
329 between microbes using imaging mass spectrometry. Fems Microbiology Reviews 40:807-813.
330 6. Sgobba E, Daguerre Y, Giampa M. 2021. Unravel the Local Complexity of Biological Environments
331 by MALDI Mass Spectrometry Imaging. International Journal of Molecular Sciences 22.
332 7. Watrous J, Roach P, Heath B, Alexandrov T, Laskin J, Dorrestein PC. 2013. Metabolic Profiling
333 Directly from the Petri Dish Using Nanospray Desorption Electrospray Ionization Imaging Mass
334 Spectrometry. Analytical Chemistry 85:10385-10391.
335 8. Li H, Balan P, Vertes A. 2016. Molecular Imaging of Growth, Metabolism, and Antibiotic
336 Inhibition in Bacterial Colonies by Laser Ablation Electrospray Ionization Mass Spectrometry.
337 Angewandte Chemie-International Edition 55:15035-15039.
338 9. Nagy G, Velickovic D, Chu RK, Carrell AA, Weston DJ, Ibrahim YM, Anderton CR, Smith RD. 2019.
339 Towards resolving the spatial metabolome with unambiguous molecular annotations in complex
340 biological systems by coupling mass spectrometry imaging with structures for lossless ion
341 manipulations. Chemical Communications 55:306-309.
342 10. Musat N, Musat F, Weber PK, Pett-Ridge J. 2016. Tracking microbial interactions with NanoSIMS.
343 Current Opinion in Biotechnology 41:114-121.
344 11. Boya CA, Fernandez-Marin H, Mejia LC, Spadafora C, Dorrestein PC, Gutierrez M. 2017. Imaging
345 mass spectrometry and MS/MS molecular networking reveals chemical interactions among
346 cuticular bacteria and pathogenic fungi associated with fungus-growing ants. Scientific Reports
347 7.

348 12. Pessotti RD, Hansen BL, Zacharia VM, Polyakov D, Traxler MF. 2019. High Spatial Resolution
349 Imaging Mass Spectrometry Reveals Chemical Heterogeneity Across Bacterial Microcolonies.
350 Analytical Chemistry 91:14818-14823.
351 13. Jens JN, Breiner DJ, Phelan VV. 2022. Spray-Based Application of Matrix to Agar-Based Microbial
352 Samples for Reproducible Sample Adherence in MALDI MSI. Journal of the American Society for
353 Mass Spectrometry 33:731-734.
354 14. Velickovic D, Chu RK, Carrell AA, Thomas M, Pasa-Tolic L, Weston DJ, Anderton CR. 2018.
355 Multimodal MSI in Conjunction with Broad Coverage Spatially Resolved MS2 Increases
356 Confidence in Both Molecular Identification and Localization. Analytical Chemistry 90:702-707.
357 15. Wu HM, Wu LK, Zhu Q, Wang JY, Qin XJ, Xu JH, Kong LF, Chen J, Lin S, Khan MU, Amjad H, Lin
358 WX. 2017. The role of organic acids on microbial deterioration in the Radix pseudostellariae
359 rhizosphere under continuous monoculture regimes. Scientific Reports 7.
360 16. Kunjapur AM, Prather KLJ. 2015. Microbial Engineering for Aldehyde Synthesis. Applied and
361 Environmental Microbiology 81:1892-1901.
362 17. Ellis EM. 2002. Microbial aldo-keto reductases. Fems Microbiology Letters 216:123-131.
363 18. Parsons JB, Yao JW, Frank MW, Jackson P, Rock CO. 2012. Membrane Disruption by
364 Antimicrobial Fatty Acids Releases Low-Molecular-Weight Proteins from Staphylococcus aureus.
365 Journal of Bacteriology 194:5294-5304.
366 19. Tran VG, Zhao HM. 2022. Engineering robust microorganisms for organic acid production.
367 Journal of Industrial Microbiology & Biotechnology 49.
368 20. Velickovic D, Lin VS, Rivas A, Anderton CR, Moran JJ. 2020. An approach for broad molecular
369 imaging of the root-soil interface via indirect matrix-assisted laser desorption/ionization mass
370 spectrometry. Soil Biology & Biochemistry 146.

371 21. Zemaitis KJ, Lin VS, Ahkami A, Winkler T, Anderton CR, Veličković D. 2023. [Preprint] Expanded
372 Coverage of Phytocompounds by Mass Spectrometry Imaging Using On-Tissue Chemical
373 Derivatization by 4-APEBA. ChemRxiv doi:https://doi.org/10.26434/chemrxiv-2023-v0xj4-v2.
374 22. Zhou QQ, Fulop A, Hopf C. 2021. Recent developments of novel matrices and on-tissue chemical
375 derivatization reagents for MALDI-MSI. Analytical and Bioanalytical Chemistry 413:2599-2617.
376 23. Larson EA, Forsman TT, Stuart L, Alexandrov T, Lee YJ. 2022. Rapid and Automatic Annotation of
377 Multiple On-Tissue Chemical Modifications in Mass Spectrometry Imaging with Metaspace.
378 Analytical Chemistry 94:8983-8991.
379 24. Sejalon-Cipolla M, Bruyat P, Bregant S, Malgorn C, Devel L, Subra G, Cantel S. 2021. Targeting
380 out of range biomolecules: Chemical labeling strategies for qualitative and quantitative MALDI
381 MS-based detection. Trac-Trends in Analytical Chemistry 143.
382 25. Bhattacharjee A, Anderson LN, Alfaro T, Porras-Alfaro A, Jumpponen A, Hofmockel KS, Jansson
383 JK, Anderton CR, Nelson WC. 2021. Draft Genome Sequence of Fusarium sp. Strain DS 682, a
384 Novel Fungal Isolate from the Grass Rhizosphere. Microbiol Resour Announc 10.
385 26. Dataset provided by Dušan Veličković, Pacific Northwest National Laboratory. Agar_NEDC, *on*
386 METASPACE. https://metaspace2020.eu/annotations?db_id=374&prj=b43e6772-d58c-11ed-
387 afbb-53f7af38ceec&ds=2023-03-13_22h46m34s. Accessed 04/27/2023.
388 27. Konopka JB. 2012. N-acetylglucosamine (GlcNAc) functions in cell signaling. Scientifica (Cairo)
389 2012.
390 28. Jung T, Mack M. 2018. Interaction of enzymes of the tricarboxylic acid cycle in Bacillus subtilis
391 and Escherichia coli: a comparative study. Fems Microbiology Letters 365.
392 29. Diomande SE, Nguyen-The C, Guinebretiere MH, Broussolle V, Brillard J. 2015. Role of fatty acids
393 in Bacillus environmental adaptation. Frontiers in Microbiology 6.

394 30. Desbois AP, Smith VJ. 2010. Antibacterial free fatty acids: activities, mechanisms of action and
395 biotechnological potential. Applied Microbiology and Biotechnology 85:1629-1642.
396 31. Andrić S, Meyer T, Ongena M. 2020. Bacillus Responses to Plant-Associated Fungal and Bacterial
397 Communities. Frontiers in Microbiology 11.
398 32. Kosono S, Tamura M, Suzuki S, Kawamura Y, Yoshida A, Nishiyama M, Yoshida M. 2015. Changes
399 in the Acetylome and Succinylome of Bacillus subtilis in Response to Carbon Source. Plos One
400 10.
401 33. Dataset provided by Dušan Veličković, Pacific Northwest National Laboratory.
402 Agar_w/o_EDC_w_4-APEBA, *on* METASPACE. https://metaspace2020.eu/annotations?ds=2023-
403 03-31_23h15m39s&viewId=sU.~Vswu. Accessed 04/27/2023.
404 34. Dataset provided by Dušan Veličković, Pacific Northwest National Laboratory.
405 Agar_w_EDC_w_4-APEBA, *on* METASPACE. https://metaspace2020.eu/annotations?ds=2023-
406 03-08_02h49m09s&viewId=tNBAag-A. Accessed 04/27/2023.
407 35. Dataset provided by Dušan Veličković, Pacific Northwest National Laboratory. Comparison of
408 Agar_w/o_EDC_w_4-APEBA and Agar_w_EDC_w_4-APEBA, *on* METASPACE.
409 https://metaspace2020.eu/datasets/2023-03-
410 31_23h15m39s/comparison?db_id=374&chem_mod=%2BN2H22C18Br&add=%5BM%5D%2B&v
411 iewId=pMCQpSSh&sort=datasetcount&row=4. Accessed 04/27/2023.
412 36. Ali NO, Bignon J, Rapoport G, Debarbouille M. 2001. Regulation of the acetoin catabolic pathway
413 is controlled by sigma L in Bacillus subtilis. Journal of Bacteriology 183:2497-2504.
414 37. Silva YP, Bernardi A, Frozza RL. 2020. The Role of Short-Chain Fatty Acids From Gut Microbiota in
415 Gut-Brain Communication. Frontiers in Endocrinology 11.
416 38. Velickovic D, Zhou MW, Schilling JS, Zhang JW. 2021. Using MALDI-FTICR-MS Imaging to Track
417 Low-Molecular-Weight Aromatic Derivatives of Fungal Decayed Wood. Journal of Fungi 7.

418 39. Lukowski JK, Bhattacharjee A, Yannarell SM, Schwarz K, Shor LM, Shank EA, Anderton CR. 2021.
419 Expanding Molecular Coverage in Mass Spectrometry Imaging of Microbial Systems Using Metal-
420 Assisted Laser Desorption/Ionization. Microbiology Spectrum 9:e00520-21.
421 40. Bhattacharjee A, Qafoku O, Richardson Jocelyn A, Anderson Lindsey N, Schwarz K, Bramer Lisa
422 M, Lomas Gerard X, Orton Daniel J, Zhu Z, Engelhard Mark H, Bowden Mark E, Nelson William C,
423 Jumpponen A, Jansson Janet K, Hofmockel Kirsten S, Anderton Christopher R. 2022. A Mineral-
424 Doped Micromodel Platform Demonstrates Fungal Bridging of Carbon Hot Spots and Hyphal
425 Transport of Mineral-Derived Nutrients. mSystems 7:e00913-22.

426

427

428

429

430

431

432

433

434

435

436

437

438

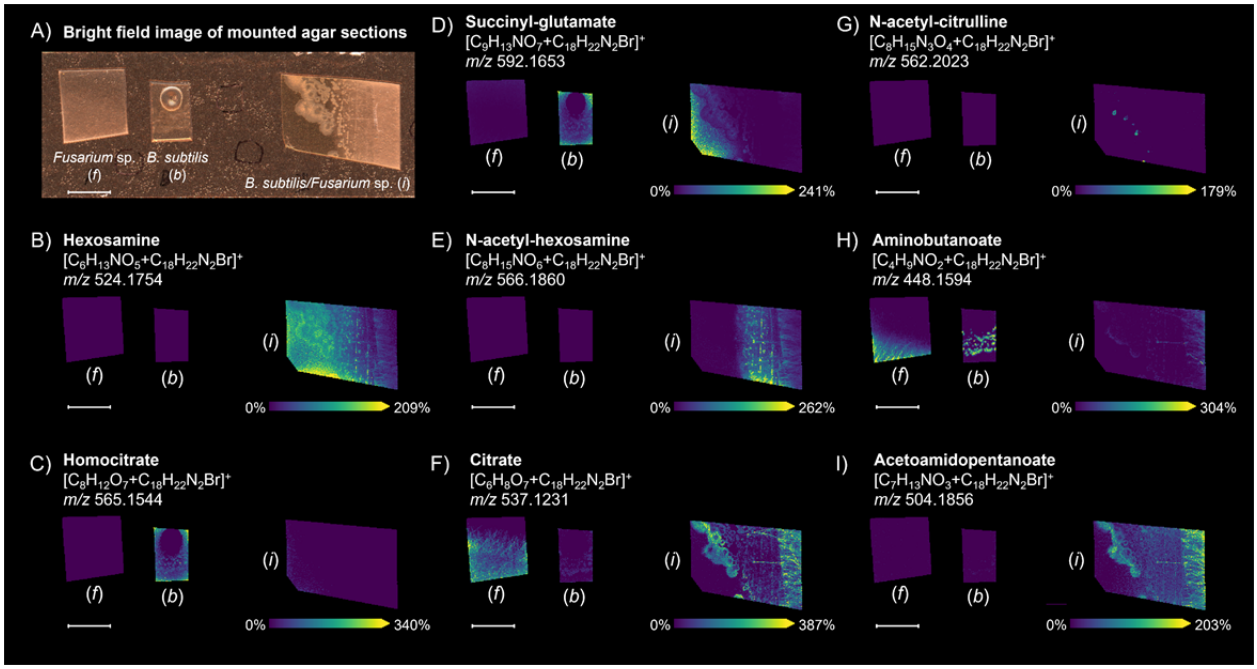

Figure 1. Characteristic patterns observed in the production and distribution of carbonyls from the interaction of *B. subtilis* and *Fusarium* sp. using the 4-APEBA-based OTCD approach. Each image is annotated with (*f*) showing the isolated *Fusarium* sp. Control, (*b*) showing the isolated *B. subtilis* control, and (*i*) showing the interaction zone of the co-culture of *B. subtilis* and *Fusarium* sp. A) An optical image of isolated colonies and the interaction of *B. subtilis* and *Fusarium* sp. Colonies on the copper tape cover slide. MALDI-MS ion images of carbonyls are highlighted that show: B) increased excretion from *B. subtilis* during interaction with *Fusarium* sp.; C) suppressed excretion from *B. subtilis* while in interaction with *Fusarium* sp.; D) no change in abundance between isolated and colonies in interaction; E) increased production in *Fusarium* sp. while in interaction with *B. subtilis*; F) increased production in *B. subtilis* and steady state in *Fusarium* sp. during interaction; G) hot spots in *B. subtilis* biofilm during interaction with *Fusarium* sp.; H) suppressed production in both *B. subtilis* and *Fusarium* sp. in interaction compared to isolated cultures; and I) increased production in both *B. subtilis* and *Fusarium* sp. in interaction compared to isolated culture. Scale bars are 7 mm and each ion images intensity is respectively scaled.

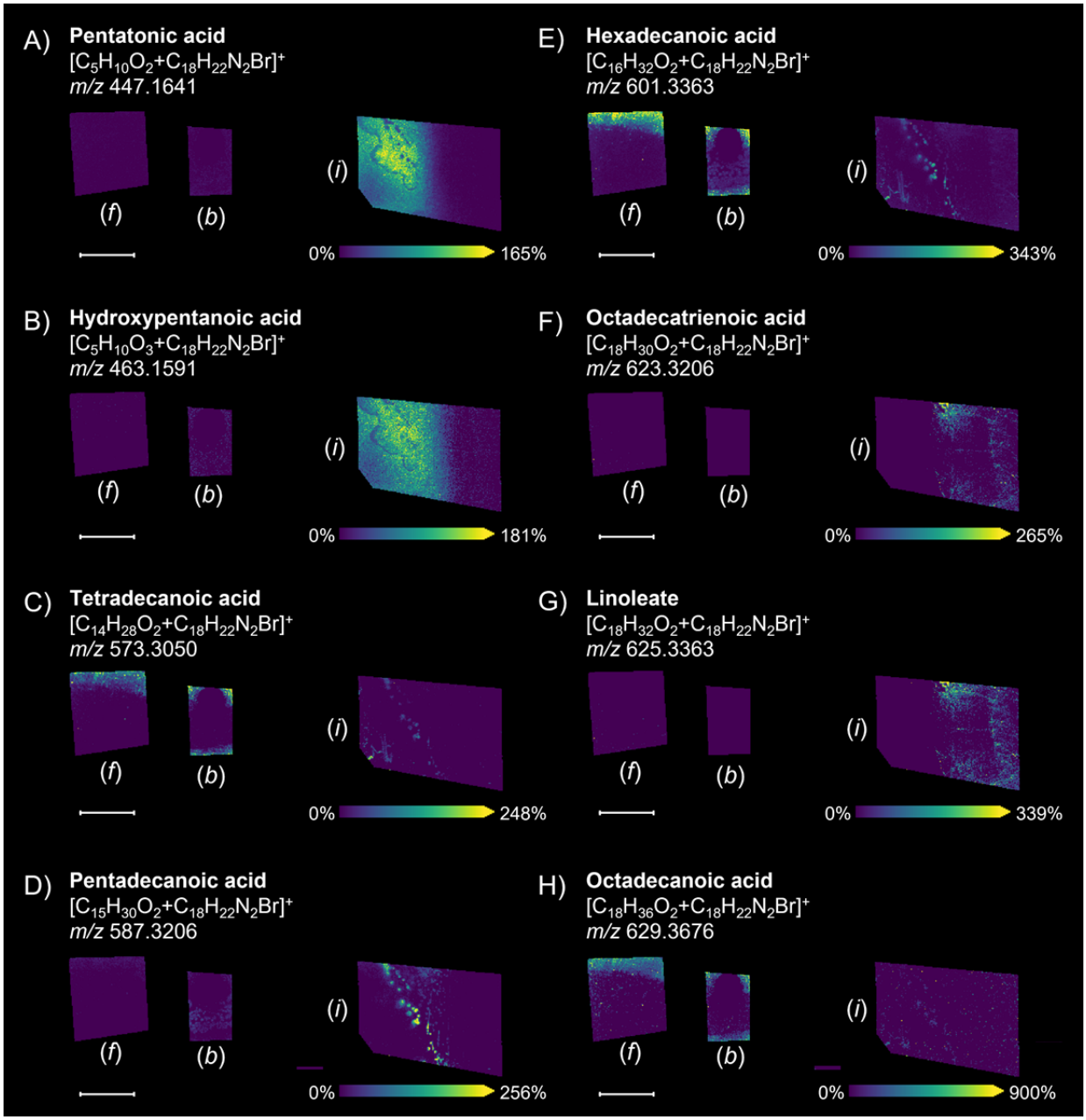

Figure 2. Shift in production and distribution of select aliphatic carboxylic acids during the *B. subtilis* and *Fusarium* sp. interaction, as well as isolated controls of each culture using the 4-APEBA-based OTCD approach. Each image is annotated with (*f*) showing the isolated *Fusarium* sp. Control, (*b*) showing the isolated *B. subtilis* control, and (*i*) showing the interaction zone of the co-culture of *B. subtilis* and *Fusarium* sp. Scale bars are 7 mm and each ion images intensity is respectively scaled.

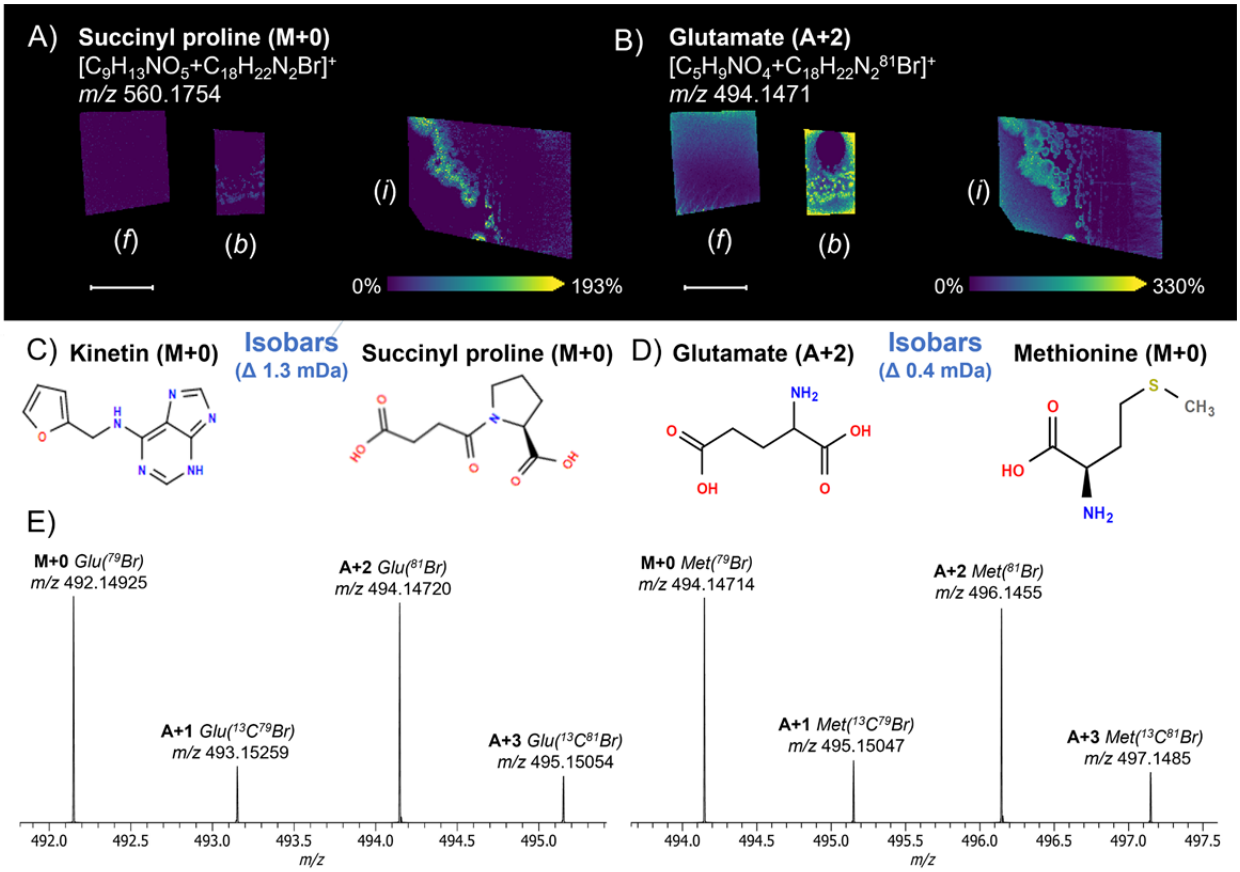

Figure 3. Resolving isobars using the 4-APEBA-based OTCD approach. Each image is annotated with (*f*) showing the isolated *Fusarium* sp. Control, (*b*) showing the isolated *B. subtilis* control, and (*i*) showing the interaction zone of the co-culture of *B. subtilis* and *Fusarium* sp. A) MALDI-MS ion images of *m/z* 560.1754 are shown with C) chemical structures of tentatively annotated derivatized isobaric metabolites monoisotopic kinetin (M+0, $C_{10}H_9N_5O+C_{18}H_{22}N_2{}^{79}Br$) and monoisotopic succinyl proline (M+0, $C_9H_{13}NO_5+C_{18}H_{22}N_2{}^{79}Br$), which differ by 1.3 mDa. Since kinetin does not contain a carbonyl that can derivatized, this confirms the annotation of succinyl proline. B) MALDI-MS ion images of *m/z* 490.1471 are shown with D) chemical structures of tentatively annotated derivatized isobaric metabolites monoisotopic methionine (M+0, $C_5H_{11}NO_2S+C_{18}H_{22}N_2{}^{79}Br$) and the second isotopologue glutamate (A+2, $C_5H_9NO_4+C_{18}N_2H_{22}{}^{81}Br$), which differ by 0.4 mDa. E) Theoretical simulations of isotopic distributions of both tentatively annotated isobars of methionine and glutamate, where within the spectra the third (A+2, ^{81}Br) and fourth isotopologue peaks (A+3, $^{13}C^{81}Br$) of methionine are not present at ratios representative of ^{79}Br and ^{81}Br isotopic distributions. This confirms methionine as a false annotation of the third isotopologue (A+2, ^{81}Br) of glutamate. Scale bars are 7 mm and each ion images intensity is respectively scaled.

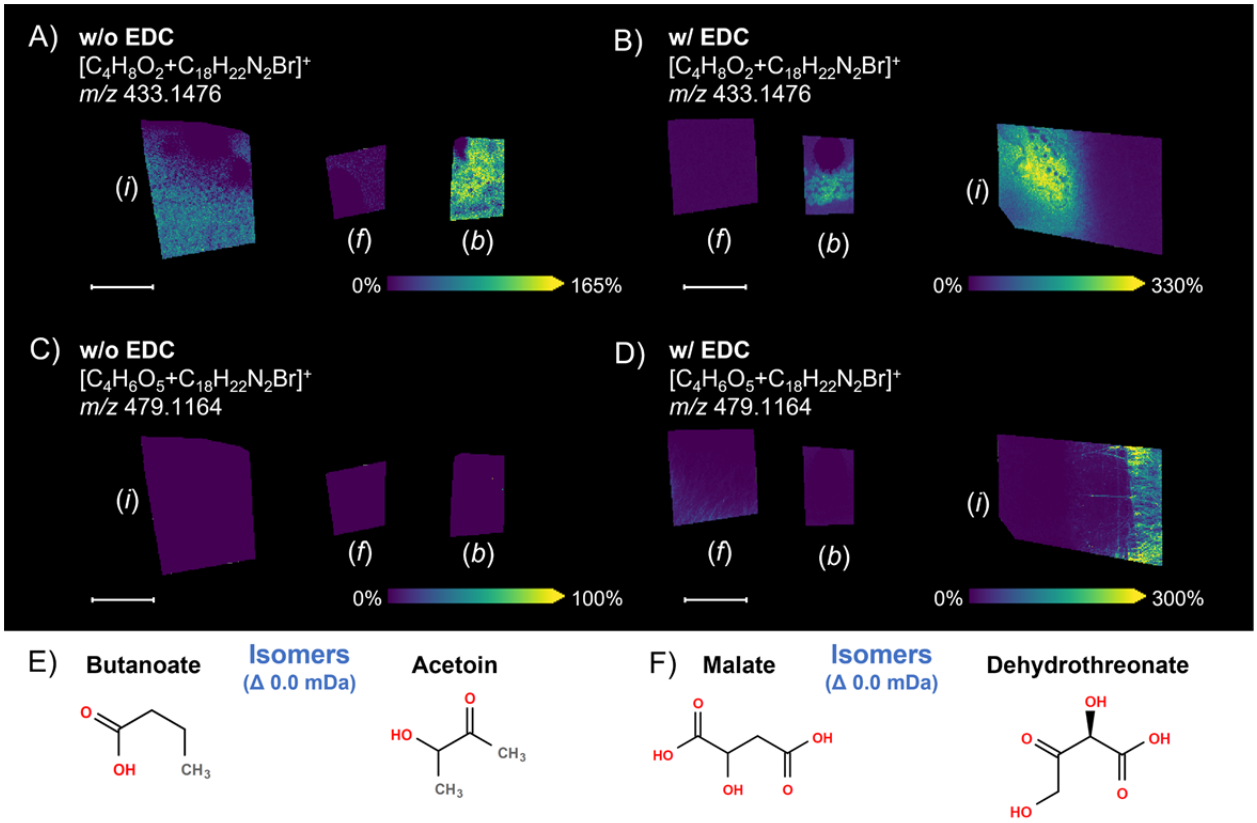

Figure 4. Resolving isomers using 4-APEBA-based OTCD with and without prior addition of EDC, which activates carboxylic acids prior to derivatization. Each image is annotated with (*f*) showing the isolated *Fusarium* sp. Control, (*b*) showing the isolated *B. subtilis* control, and (*i*) showing the interaction zone of the co-culture of *B. subtilis* and *Fusarium* sp.. MALDI-MS ion images from samples which underwent preparation A) without EDC and B) with EDC are shown for *m/z* 433.1476. Additional MALDI-MS ion images of *m/z* 479.1164 are shown C) without EDC and D) with EDC. Here, the ion at *m/z* 479.1164 was not detected within C) without prior activation of carboxylic acids with EDC. E) The molecular structures of two tentatively annotated isomers, butanoic acid (carboxylic acid) and acetoin (ketone), are possible annotations for *m/z* 433.1476. F) The molecular structures of the other two tentatively annotated isomers, malate (solely carboxylic acid) and dehydrothreonate (oxoacid) are depicted for annotations at *m/z* 479.1164. Scale bars are 7 mm and each ion images intensity is respectively scaled.

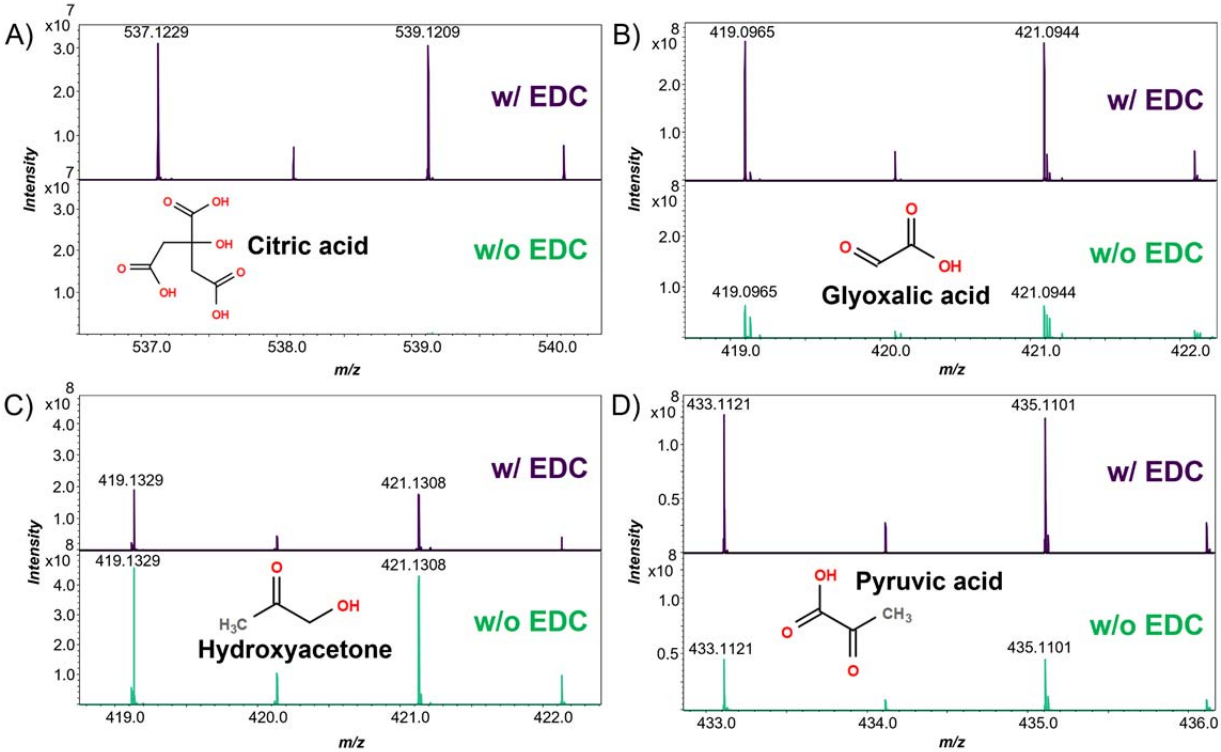

Figure 5. MALDI mass spectra of carbonyl standards with and without EDC activation prior to 4-APEBA derivatization. Mass spectra are shown for A) citric acid as a model carboxylic acid, B) glyoxalic acid as an oxocarboxylic acid with an aldehyde, C) hydroxyacetone as an oxoacid with a ketone, and D) pyruvic acid as an oxocarboxylic acid with a ketone. Peaks that correspond the monoisotopic (M+0, ^{79}Br) and second isotopologue (A+2, ^{81}Br) were annotated and shown in each spectrum and the structure of each metabolite is also presented.

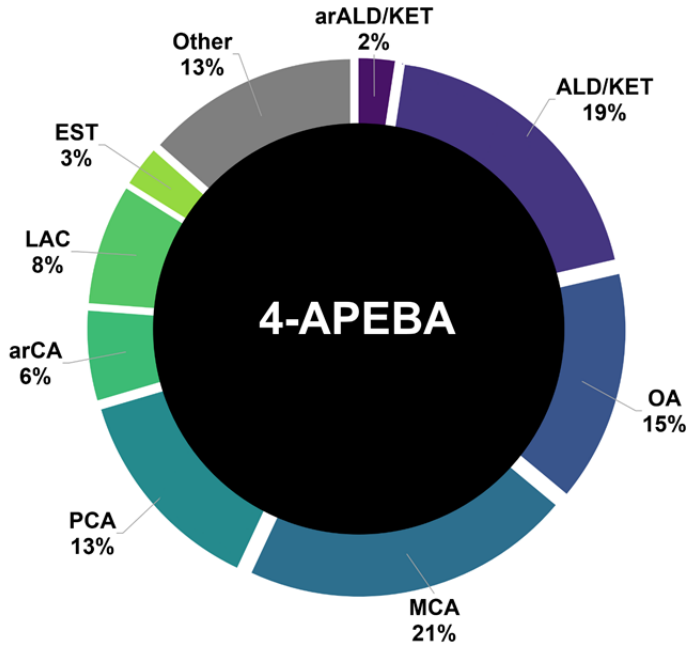

Abbreviation	Label
arALD/KET	aromatic aldehydes/ketones
ALD/KET	aldehydes/ketones
OA	oxoacids
MCA	monocartboxylic acids
PCA	polycarboxylic acids
arCA	aromatic carboxylic acids
LAC	lactones
EST	esters
Other	others

Supplementary Figure S1. The breakdown of the carbonyl classes of the 316 assigned spectral peaks which underwent discriminate analysis within **Table S1** is shown. Here all annotations from KEGG-v1 output from METASPACE were bulked into representative carbonyl types, and then represented as a total percent of all bulked annotations of carbonyl type.

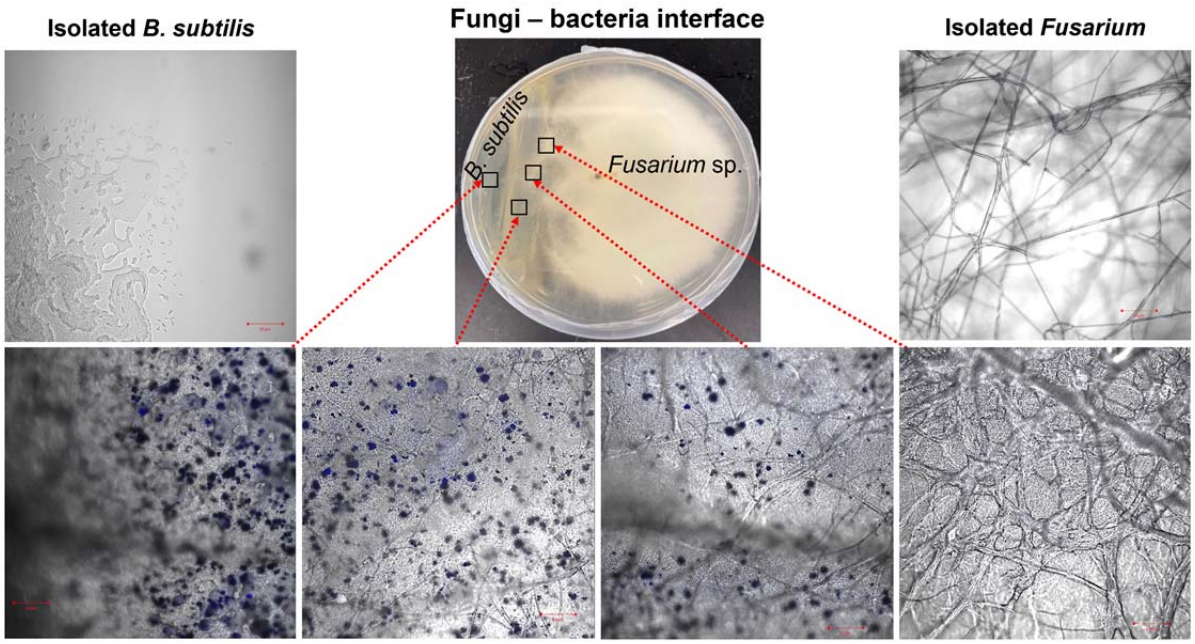

Supplementary Figure S2. Optical microscopy images highlight microbial pigments produced as a result of fungi-bacteria interactions. Fungal hyphal architecture changes in presence of bacteria as shown in the inset zoomed views for the interaction zone (bottom panel) compared to isolated *B. subtilis* (top left) and *Fusarium* sp. (top right), all scale bars are 50 µm.

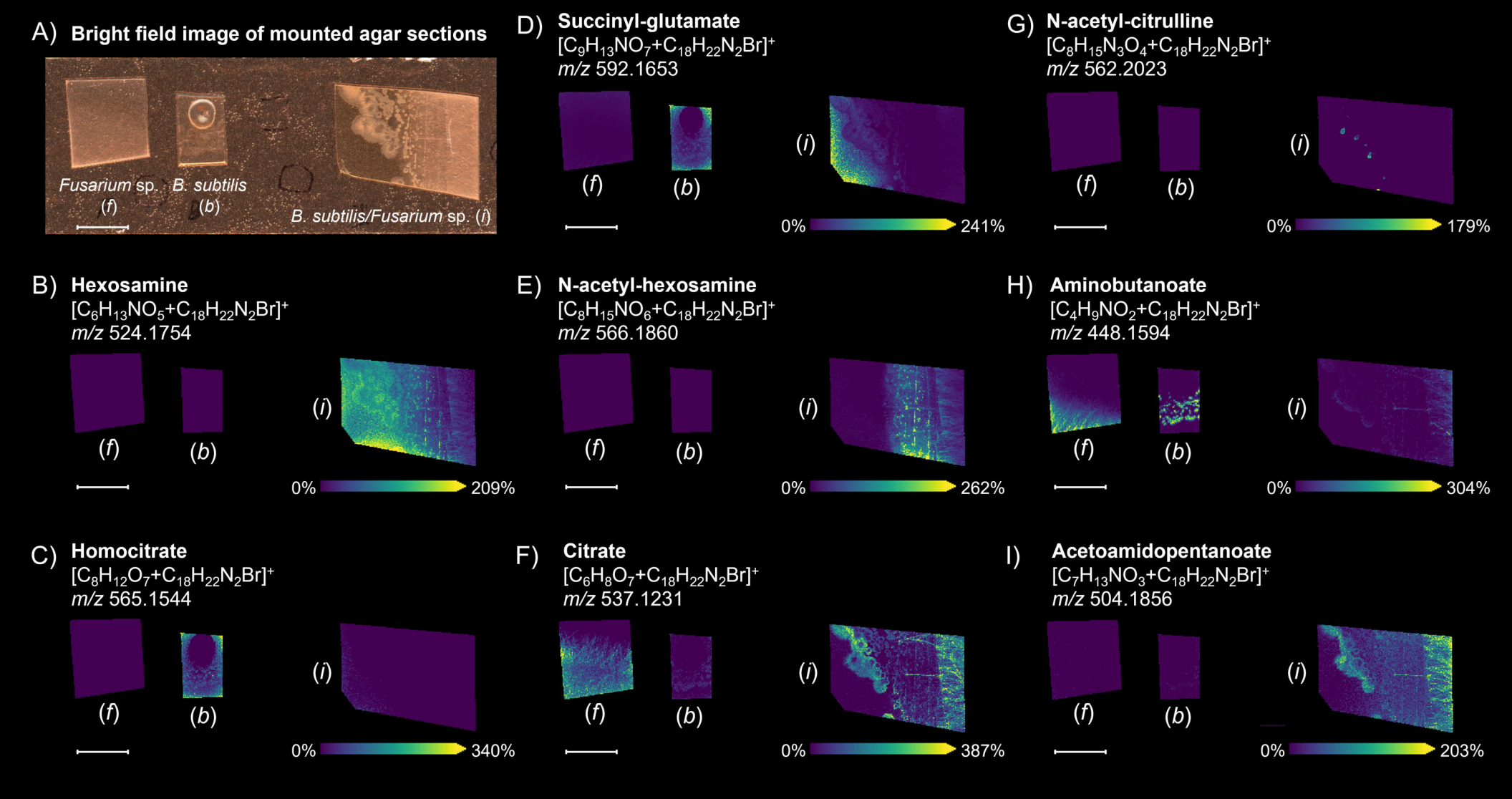
A) Bright field image of mounted agar sections
Fusarium sp. (f)
B. subtilis (b)
B. subtilis/Fusarium sp. (i)
B) Hexosamine
[C6H13NO5+C18H22N2Br]+
m/z 524.1754
(f)
(b)
(i)
0%
209%
C) Homocitrate
[C8H12O7+C18H22N2Br]+
m/z 565.1544
(f)
(b)
(i)
0%
340%
D) Succinyl-glutamate
[C9H13NO7+C18H22N2Br]+
m/z 592.1653
(f)
(b)
(i)
0%
241%
E) N-acetyl-hexosamine
[C8H15NO6+C18H22N2Br]+
m/z 566.1860
(f)
(b)
(i)
0%
262%
F) Citrate
[C6H8O7+C18H22N2Br]+
m/z 537.1231
(f)
(b)
(i)
0%
387%
G) N-acetyl-citrulline
[C8H15N3O4+C18H22N2Br]+
m/z 562.2023
(f)
(b)
(i)
0%
179%
H) Aminobutanoate
[C4H9NO2+C18H22N2Br]+
m/z 448.1594
(f)
(b)
(i)
0%
304%
I) Acetoamidopentanoate
[C7H13NO3+C18H22N2Br]+
m/z 504.1856
(f)
(b)
(i)
0%
203%

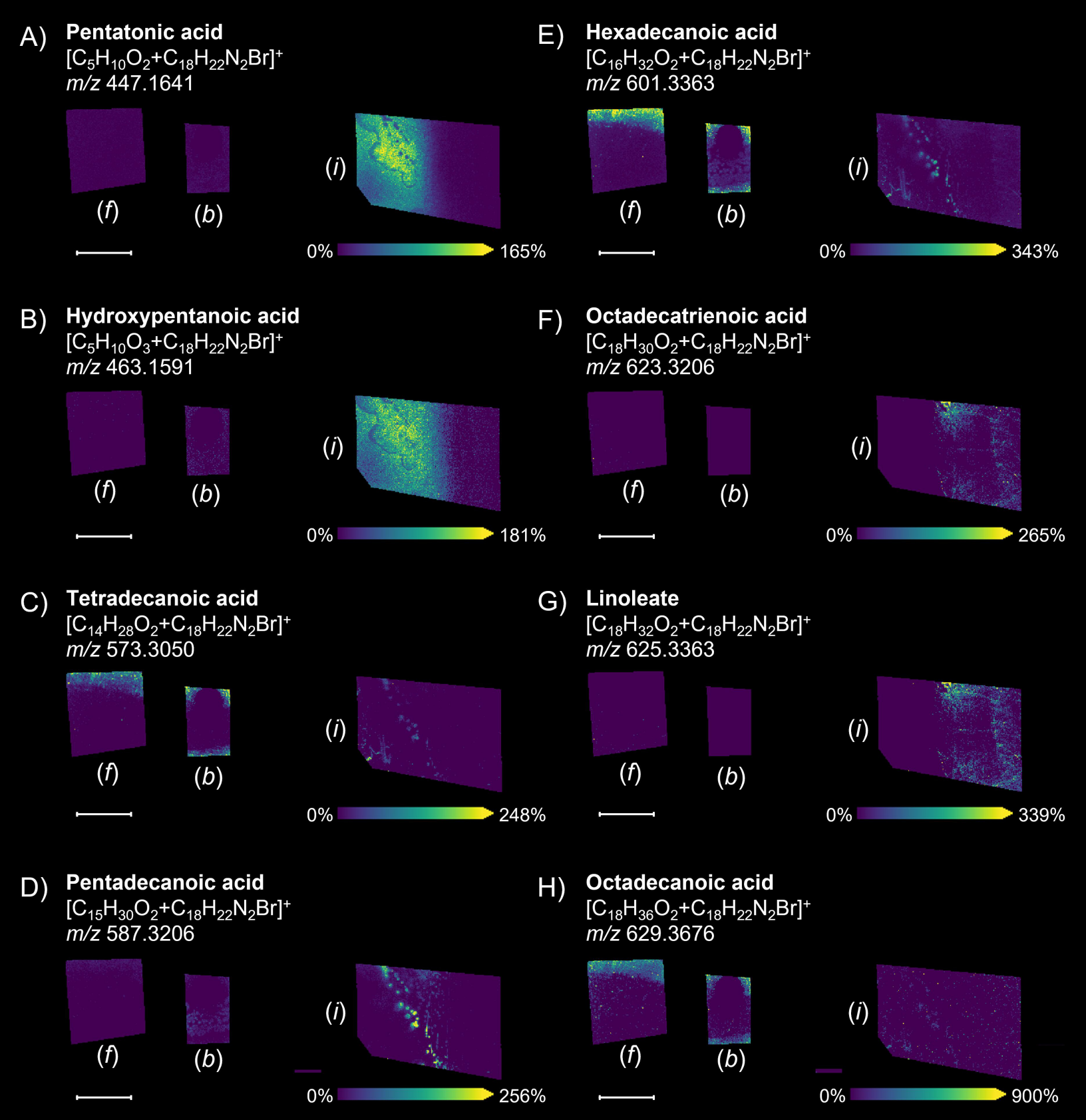
A)
Pentatonic acid
[C5H10O2+C18H22N2Br]+
m/z 447.1641
(f)
(b)
(i)
0%
165%
B)
Hydroxypentanoic acid
[C5H10O3+C18H22N2Br]+
m/z 463.1591
(f)
(b)
(i)
0%
181%
C)
Tetradecanoic acid
[C14H28O2+C18H22N2Br]+
m/z 573.3050
(f)
(b)
(i)
0%
248%
D)
Pentadecanoic acid
[C15H30O2+C18H22N2Br]+
m/z 587.3206
(f)
(b)
(i)
0%
256%
E)
Hexadecanoic acid
[C16H32O2+C18H22N2Br]+
m/z 601.3363
(f)
(b)
(i)
0%
343%
F)
Octadecatrienoic acid
[C18H30O2+C18H22N2Br]+
m/z 623.3206
(f)
(b)
(i)
0%
265%
G)
Linoleate
[C18H32O2+C18H22N2Br]+
m/z 625.3363
(f)
(b)
(i)
0%
339%
H)
Octadecanoic acid
[C18H36O2+C18H22N2Br]+
m/z 629.3676
(f)
(b)
(i)
0%
900%

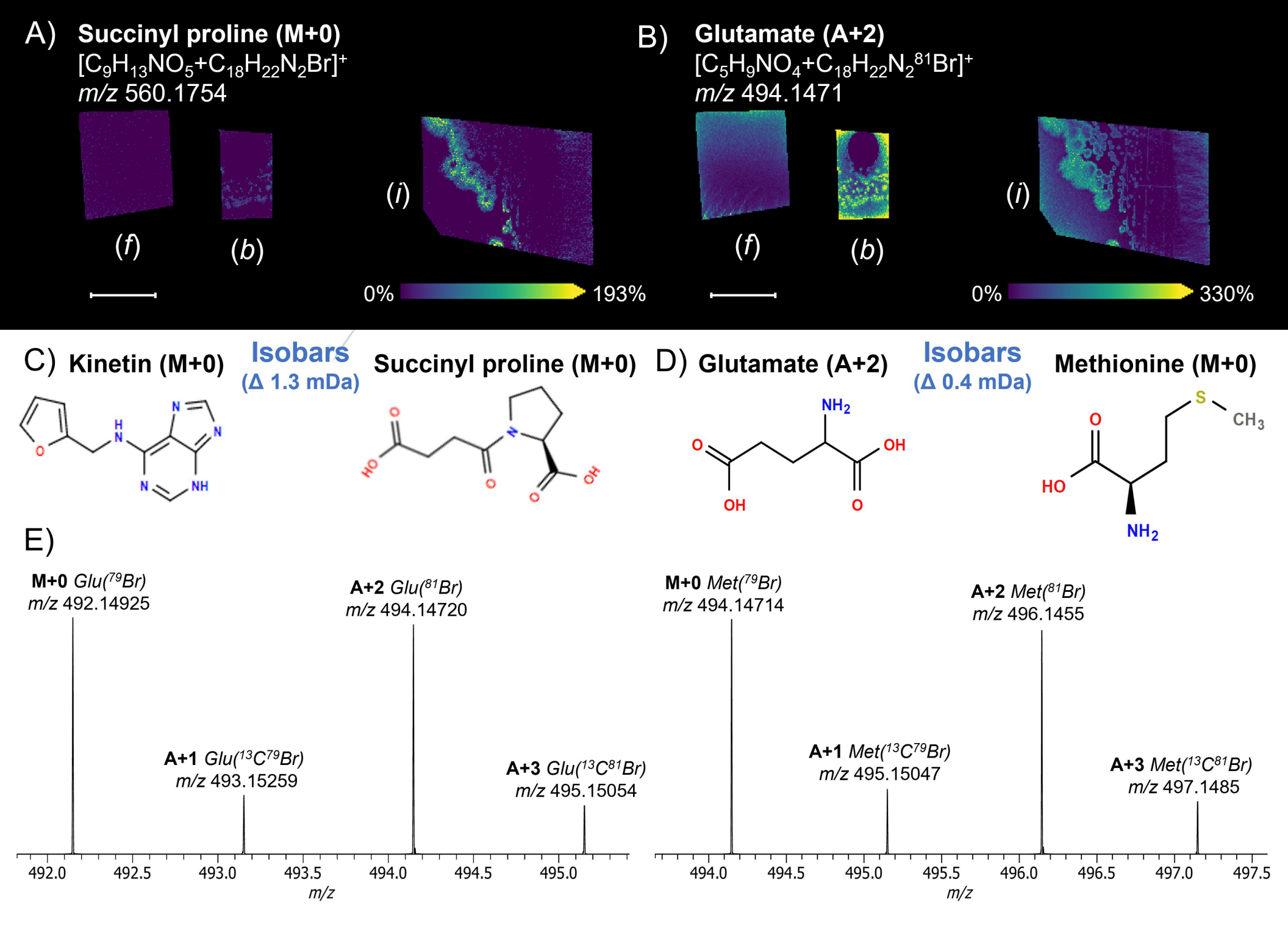
A) Succinyl proline (M+0)
[C9H13NO5+C18H22N2Br]+
m/z 560.1754
(f)
(b)
(i)
0%
193%
B) Glutamate (A+2)
[C5H9NO4+C18H22N2 81Br]+
m/z 494.1471
(f)
(b)
(i)
0%
330%
C) Kinetin (M+0)
Isobars
(Δ 1.3 mDa)
Succinyl proline (M+0)
D) Glutamate (A+2)
Isobars
(Δ 0.4 mDa)
Methionine (M+0)
E)
M+0 Glu(79Br)
m/z 492.14925
A+1 Glu(13C79Br)
m/z 493.15259
A+2 Glu(81Br)
m/z 494.14720
A+3 Glu(13C81Br)
m/z 495.15054
492.0
492.5
493.0
493.5
494.0
494.5
495.0
m/z
M+0 Met(79Br)
m/z 494.14714
A+1 Met(13C79Br)
m/z 495.15047
A+2 Met(81Br)
m/z 496.1455
A+3 Met(13C81Br)
m/z 497.1485
494.0
494.5
495.0
495.5
496.0
496.5
497.0
497.5
m/z

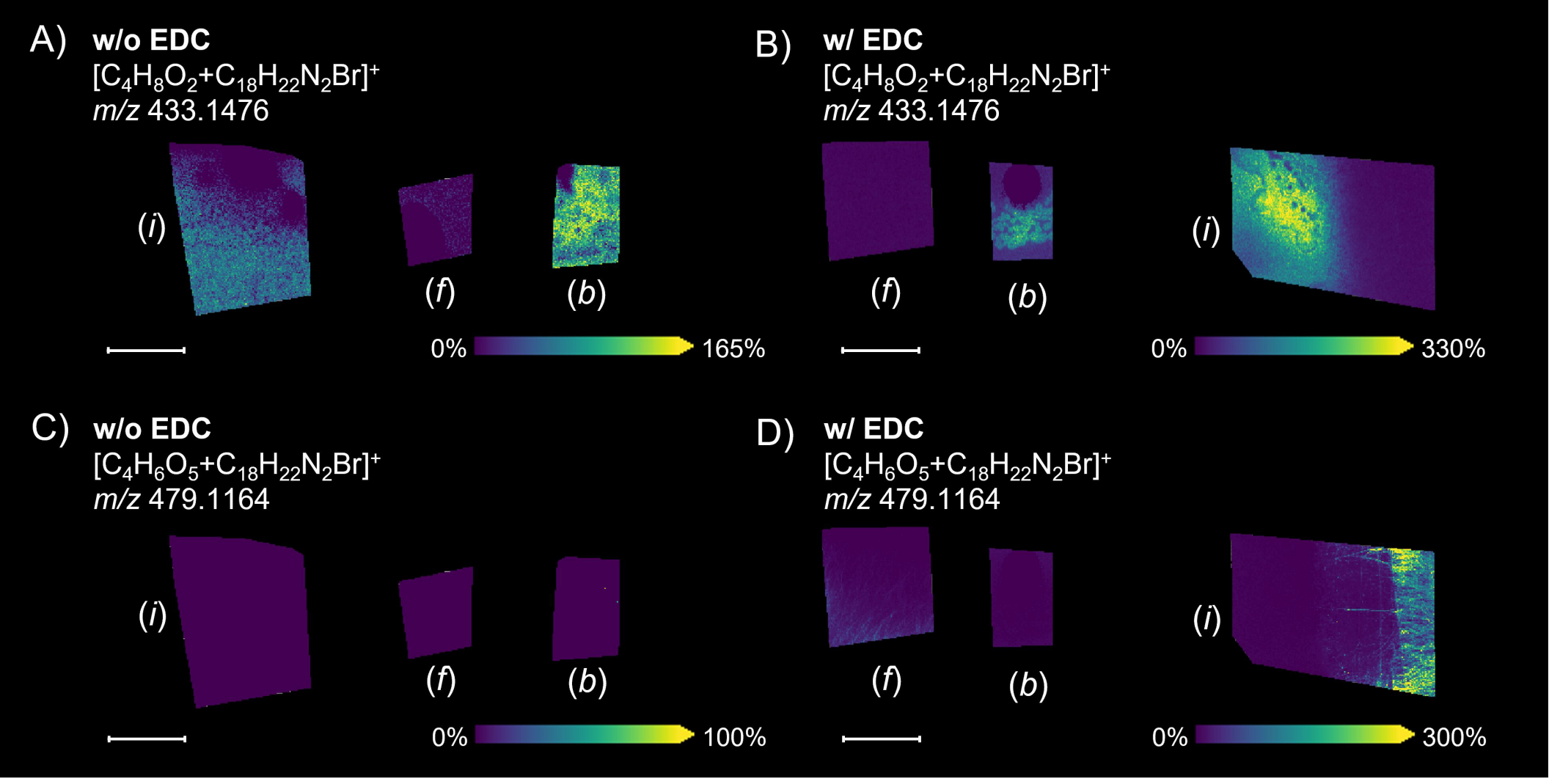

E) **Butanoate** **Isomers** (Δ 0.0 mDa) **Acetoin**

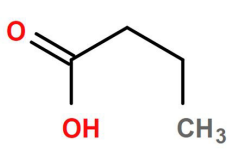

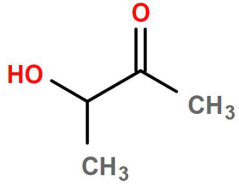

F) **Malate** **Isomers** (Δ 0.0 mDa) **Dehydrothreonate**

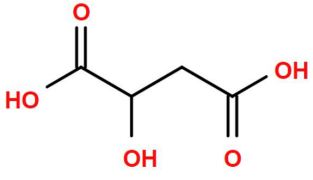

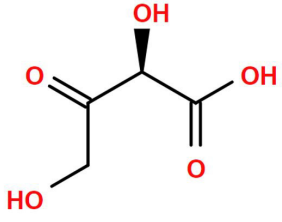

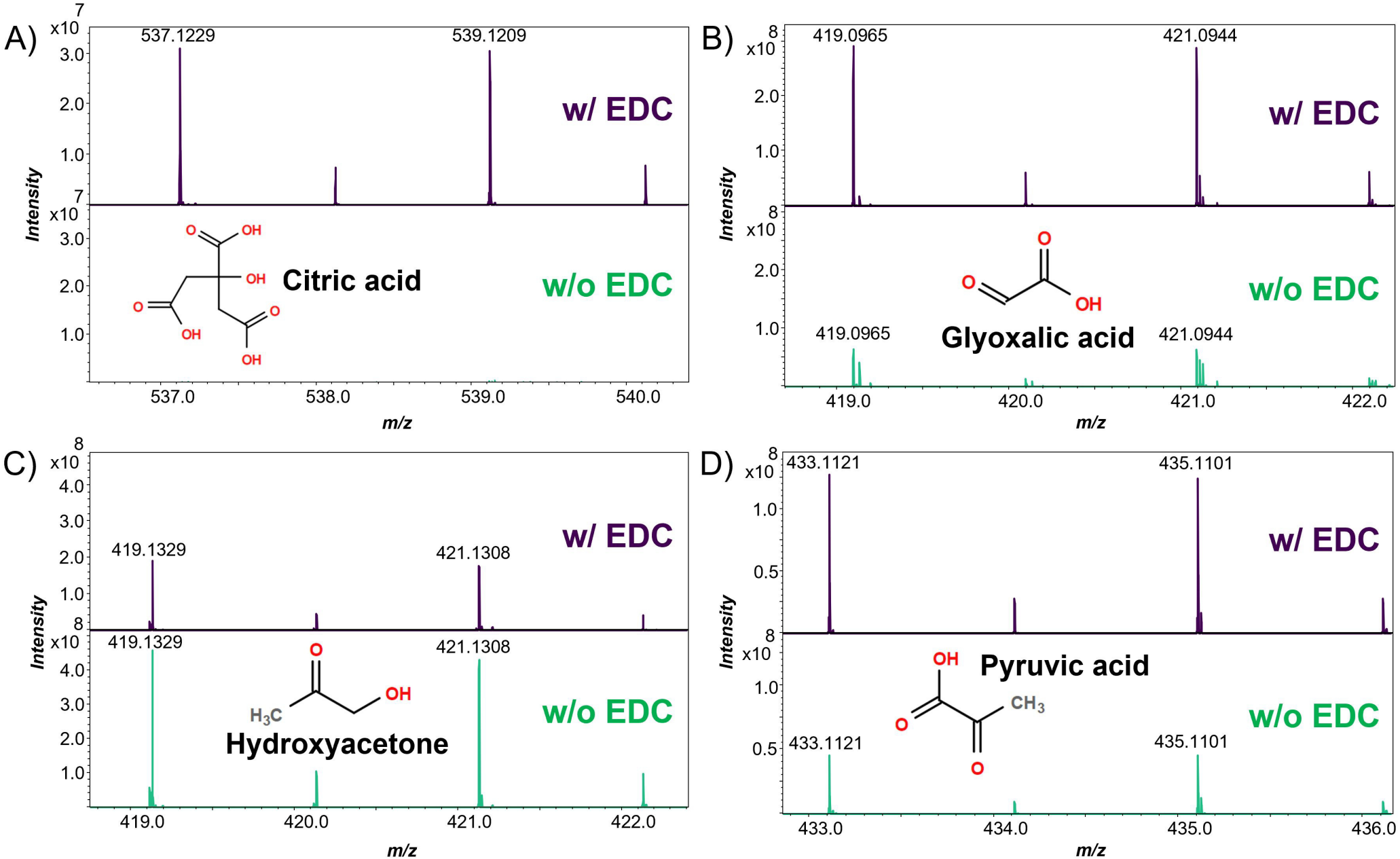
A)
537.1229
539.1209
w/ EDC
w/o EDC
Citric acid
Intensity
m/z
B)
419.0965
421.0944
w/ EDC
w/o EDC
Glyoxalic acid
C)
419.1329
421.1308
w/ EDC
w/o EDC
Hydroxyacetone
D)
433.1121
435.1101
w/ EDC
w/o EDC
Pyruvic acid

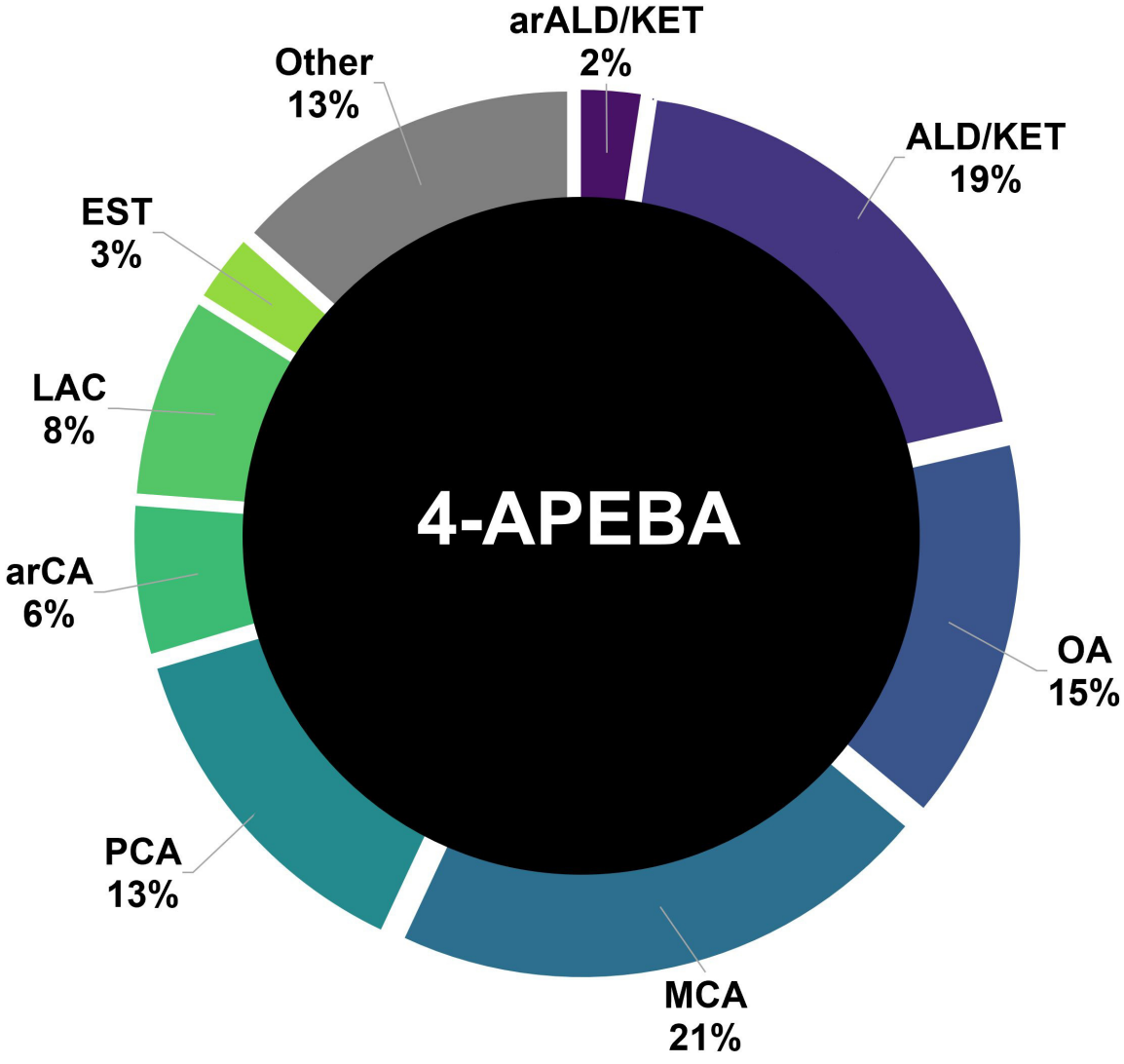

Abbreviation	Label
arALD/KET	aromatic aldehydes/ketones
ALD/KET	aldehydes/ketones
OA	oxoacids
MCA	monocartboxylic acids
PCA	polycarboxylic acids
arCA	aromatic carboxylic acids
LAC	lactones
EST	esters
Other	others

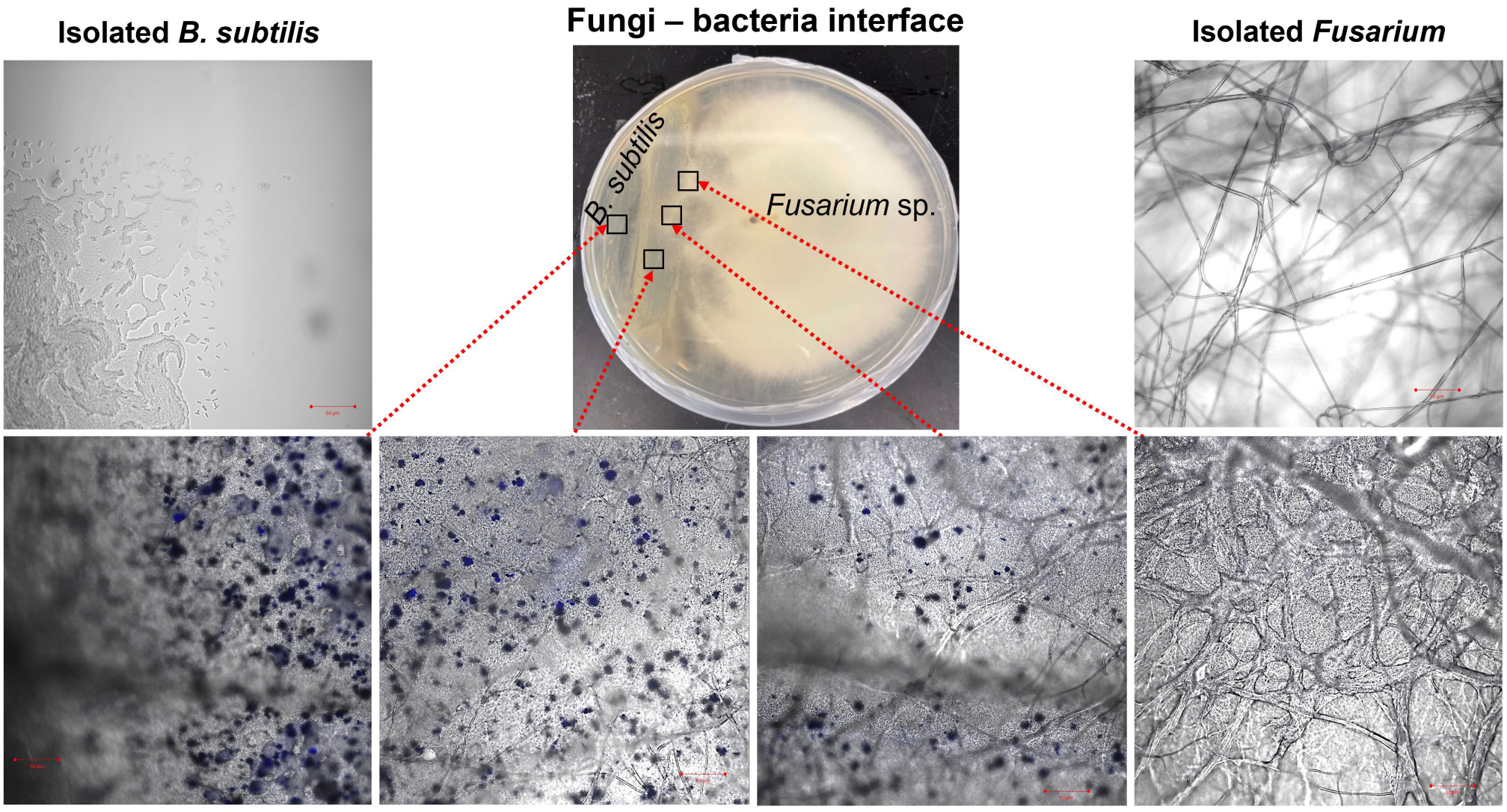
Isolated *B. subtilis*
Fungi – bacteria interface
Isolated *Fusarium*
B. subtilis
Fusarium sp.